Nuclear shape dependence of Gamow-Teller distributions in neutron-deficient Pb isotopes

P. Sarriguren, O. Moreno, R. Álvarez-Rodríguez, and E. Moya de Guerra
Instituto de Estructura de la Materia, Consejo Superior de Investigaciones Científicas, Serrano 123, E-28006 Madrid, Spain
(February 6, 2008)

We study Gamow-Teller strength distributions in the neutron-deficient even isotopes $^{184-194}$Pb in a search for signatures of deformation. The microscopic formalism used is based on a deformed quasiparticle random phase approximation (QRPA) approach, which involves a self-consistent quasiparticle deformed Skyrme Hartree-Fock (HF) basis and residual spin-isospin forces in both the particle-hole and particle-particle channels. By analyzing the sensitivity of the Gamow-Teller strength distributions to the various ingredients in the formalism, we conclude that the β-decay of these isotopes could be a useful tool to look for fingerprints of nuclear deformation.

PACS: 21.60.Jz, 23.40.-s, 27.70.+q, 27.80.+w

I. INTRODUCTION

Neutron-deficient Pb isotopes turn out to be a unique laboratory to explore the phenomenon of shape coexistence in nuclei and have recently been a subject of much experimental and theoretical interest. The existence of at least one low-lying excited 0^+ state in all even-even Pb isotopes between $A = 184$ and $A = 194$ has been experimentally observed at excitation energies below 1 MeV (see Ref. [1] and references therein). The most extreme cases are ^{186}Pb and ^{188}Pb with two excited 0^+ states below 700 keV [2,3]. These are good examples where the ground state and the first two excited states, which are below 1 MeV, correspond to macroscopical shapes. Experimental data on the excited states of these Pb isotopes are not just limited to a few 0^+ states. Rotational bands built on top of these 0^+ states have also been observed [1,4], whose properties have been used to interpret them as corresponding to oblate and prolate deformations.

The existence of the 0^+ low-lying states arises from the combined effect of a proton shell gap at $Z = 82$ and a large number of hole neutrons in the $N = 126$ core. The influence of the magic proton number $Z = 82$ is particularly strong and the ground state of Pb isotopes is known to be spherical down to ^{182}Pb. The weakening of the magicity of the $Z = 82$ shell manifests itself through the appearance of low-lying 0^+ states.

Different types of models have been invoked to explain the coexistence of several 0^+ states at low energies. In a shell model picture, the excited 0^+ states are interpreted as two-quasiparticle and four-quasiparticle configurations [5]. Protons and neutrons outside the inert core interact through pairing and quadrupole interactions to generate deformed structures. Within a mean field approach, this is interpreted as a macroscopic change from a spherical to a deformed shape. The energy of the different shape configurations can be calculated using a nuclear potential, where the energies of the single particle orbitals depend on the deformation. Potential energy surface calculations have become more and more sophisticated with time, resulting in accurate descriptions of the nuclear shapes and the configurations involved. Calculations based on phenomenological mean fields and Strutinsky method [6,7], predict the existence of several competing minima in the deformation energy surface of neutron-deficient Pb isotopes. Self-consistent mean field calculations [8,9] and calculations including correlations beyond mean field [10–12] confirm these results.

Sophisticated configuration mixing calculations [10–12] have been shown to support the mean field result that these neutron deficient systems display more than one minimum corresponding to spherical and deformed shapes. The lowest excited states in configuration mixing calculations have average deformations close to the deformation of the mean field minima [10–12]. All the approaches analyzed in Ref. [11] from mean field up to very sophisticated angular momentum projected generator coordinate method with Gogny forces provide the same underlying basic picture of strong coexisting spherical, oblate and prolate shapes. Although the mean field approach does not reproduce quantitatively the experimental relative energies of the 0^+ states, it provides a good qualitative description of the three minima and is a good approximation to associate the 0^+ states observed at low energies with coexisting energy minima in the energy surface. The physical 0^+ observed states have been also considered [13] as superpositions of spherical, oblate or prolate configurations, with relative weights determined phenomenologically, in the spirit of the shape mixing picture [13]. Such kind of calculations have been done in Ref. [14] for $^{190-200}$Pb isotopes.

Mean field predictions of deformed ground states in the neutron-deficient Pb region are very sensitive to fine details in the calculations, specially to pairing effects. This has been shown for example within deformed relativistic mean field (RMF) calculations. Standard RMF calculations [9,15] do not reproduce the spherical ground states in this mass region, being at variance with experimental data. In RMF, the ground states of neutron-deficient Pb isotopes are found to be deformed for standard forces with constant pairing gaps [16]. However, it has been shown [17] that using constant strengths for the pairing interaction (which makes the gap parameters strongly dependent on deformation), produces spherical ground states for all Pb isotopes. More recently [9], an improved pairing treatment has been used by means of relativistic Hartree-Bogoliubov (RHB) calculations, using the NL3 effective interaction and a finite range Gogny interaction to describe the pairing properties. The results of these calculations show that ^{184}Pb and ^{186}Pb have spherical ground states with low-lying oblate and prolate minima in qualitative agreement with experiment. However, with increasing neutron number, the oblate minimum is lowered in energy and $^{188-194}$Pb have oblate ground states, contradicting the experimental data [1]. In order to recover the spherical ground states, a new parametrization of the effective interaction was proposed, which takes into account the sizes of spherical shell gaps.

The special sensitivity of the ground states in this mass region to deformation and pairing effects has been also studied from non-relativistic mean field calculations. In Ref. [18] it was found that the potential energy curves in neutron-deficient Pb isotopes are very sensitive to the relative intensity of the neutron versus proton pairing strengths. In this reference it was shown that slightly different choices of the pairing strengths produce different ground state shapes.

On the other hand, it has been shown [19,20] that the decay properties of unstable nuclei may depend on the nuclear shape of the decaying parent nucleus. In particular, the Gamow-Teller (GT) strength distributions corresponding to β^+-decay of proton-rich nuclei in the mass region $A \approx 70$ has been studied systematically [20] as a function of the deformation, using a deformed HF+BCS+QRPA approach. In Ref. [20] the GT strength distributions of several nuclei were identified to be particularly sensitive to the deformation of the β^+-emitter, and a comparison of the theoretical results with recent accurate measurements [21] has been used to determine the nuclear shape in neutron deficient Kr and Sr isotopes.

In this paper we study the GT strength distributions of neutron-deficient Pb isotopes from $A = 184$ up to $A = 194$ and their dependence on deformation. The aim here is to identify possible signatures that allow one to determine the existence of spherical, prolate or oblate nuclear shapes, in the spirit of the shape coexistence picture, by looking at the β^+-decay pattern. Although possible effects of the quadrupole shape mixing cannot be discarded and a QRPA-type approach might not be a good approximation to treat systems undergoing large amplitude collective motions, the calculations performed in this paper are perfectly reasonable as a first estimate of the β^+-decay patterns. This study is timely because the possibility to carry out these measurements is being considered at present [22].

The paper is organized as follows. In Sec. II we present a summary of the theoretical framework used in our calculation. Sec. III contains our results on the Gamow-Teller strength distributions of the Pb isotopes, as well as a discussion of their dependence on deformation. The conclusions are written in Sec. IV.

II. THEORETICAL FRAMEWORK

In this Section we summarize briefly the theory involved in the microscopic calculations. More details can be found in Ref. [20]. The theoretical formalism used here is based on a deformed Hartree-Fock mean field calculation, using an effective two-body Skyrme interaction and including pairing correlations in BCS approximation. The single particle energies, wave functions, and occupation probabilities are generated from this mean field. We consider in this paper the force Sk3 [23], as an example of one of the most simple, traditional and successful Skyrme interaction and the force SG2 [24], which has been successfully tested against spin and isospin excitations in spherical [24] and deformed nuclei [20,25]. Some results will also be given for the more recent force SLy4 [26].

The formalism is safely restricted to axially deformed nuclear shapes because it has been shown [6,12] that no features of particular interest, such as minima or flat regions, appear for triaxial shapes in neutron-deficient Pb isotopes. Time reversal and axial symmetry are then assumed here. The single-particle wave functions are expanded in terms of the eigenstates of an axially symmetric harmonic oscillator in cylindrical coordinates, using eleven major shells. We calculate the energy surfaces as a function of deformation for all the even-even neutron-deficient Pb isotopes under study here. For that purpose, we perform constrained HF calculations with a quadrupole constraint [27] and minimize the HF energy under the constraint of keeping fixed the nuclear deformation. In order to study the above mentioned sensitivity of the energy surfaces to pairing correlations, we compare the results obtained using fixed gap parameters for protons and neutrons with the results obtained using constant pairing strengths $G_{\pi,\nu}$. The fixed gap parameters are determined phenomenologically from the odd-even mass differences [28] when this experimental information is available, otherwise, we use the expression $\Delta = 12A^{-1/2}$ MeV. The $G_{\pi,\nu}$ strengths are determined from

the expression

$$G_{\pi(\nu)} = \frac{18}{11 + Z(N)}\,\text{MeV}. \tag{2.1}$$

To describe Gamow-Teller excitations we use the QRPA adding to the mean field a separable spin-isospin residual interaction, which is expected to be the most relevant interaction for that purpose. This interaction contains two parts, particle-hole (ph) and particle-particle (pp). The ph part is responsible for the position and structure of the GT resonance [20,29–31] and it is a common practice to fit the strength of the force to reproduce the energy of the resonance [31]. The advantage of using separable forces is that the QRPA energy eigenvalue problem is reduced to find the roots of an algebraic equation. The particle-particle interaction is a neutron-proton pairing force in the $J^\pi = 1^+$ coupling channel. We introduce this interaction in the usual way [30,32,33], that is, in terms of a separable force with a coupling constant κ_{GT}^{pp}, which is fitted to the phenomenology. Since the peak of the GT resonance is almost insensitive to the pp force, κ_{GT}^{pp} is usually adjusted to reproduce the half-lives [30,31].

The pnQRPA phonon operator for GT excitations in even-even nuclei is written as

$$\Gamma^+_{\omega_K} = \sum_{\pi\nu} \left[X^{\omega_K}_{\pi\nu} \alpha^+_\nu \alpha^+_{\bar{\pi}} - Y^{\omega_K}_{\pi\nu} \alpha_{\bar{\nu}} \alpha_\pi \right] , \tag{2.2}$$

where π and ν stand for proton and neutron, respectively, α^+ (α) are quasiparticle creation (annihilation) operators, ω_K are the RPA excitation energies, and $X^{\omega_K}_{\pi\nu}, Y^{\omega_K}_{\pi\nu}$ the forward and backward amplitudes, respectively. It satisfies

$$\Gamma_{\omega_K} |0\rangle = 0\,; \qquad \Gamma^+_{\omega_K} |0\rangle = |\omega_K\rangle\,. \tag{2.3}$$

Solving the pnQRPA equations [29,32], the GT transition amplitudes in the intrinsic frame of even-even nuclei connecting the QRPA ground state of the parent nucleus $|0\rangle$ to one phonon states in the daughter nucleus $|\omega_K\rangle$, are given by

$$\left\langle \omega_K | \beta^\pm_K | 0 \right\rangle = \mp M^{\omega_K}_\pm \,, \tag{2.4}$$

where $\beta^\pm_K = \sigma_K t^\pm, \quad K = 0, \pm 1$, and

$$M^{\omega_K}_- = \sum_{\pi\nu} \left(q_{\pi\nu} X^{\omega_K}_{\pi\nu} + \tilde{q}_{\pi\nu} Y^{\omega_K}_{\pi\nu} \right) ; \qquad M^{\omega_K}_+ = \sum_{\pi\nu} \left(\tilde{q}_{\pi\nu} X^{\omega_K}_{\pi\nu} + q_{\pi\nu} Y^{\omega_K}_{\pi\nu} \right) , \tag{2.5}$$

with

$$\tilde{q}_{\pi\nu} = u_\nu v_\pi \Sigma^{\nu\pi}_K; \quad q_{\pi\nu} = v_\nu u_\pi \Sigma^{\nu\pi}_K\,; \qquad \Sigma^{\nu\pi}_K = \left\langle \nu \left| \sigma_K \right| \pi \right\rangle \,, \tag{2.6}$$

where v's are occupation amplitudes ($u^2 = 1 - v^2$).

Once the intrinsic amplitudes in Eq. (2.4) are calculated, the Gamow-Teller strength $B(GT)$ in the laboratory frame for a transition $I_i K_i (0^+ 0) \rightarrow I_f K_f (1^+ K)$ can be obtained as

$$B^\pm(GT) = \sum_{M_i, M_f, \mu} \left| \left\langle I_f M_f \left| \beta^\pm_\mu \right| I_i M_i \right\rangle \right|^2 = \left\{ \delta_{K_f,0} \left\langle \phi_{K_f} \left| \beta^\pm_0 \right| \phi_0 \right\rangle^2 + 2\delta_{K_f,1} \left\langle \phi_{K_f} \left| \beta^\pm_1 \right| \phi_0 \right\rangle^2 \right\} , \tag{2.7}$$

in units of $g_A^2/4\pi$. To obtain this expression we have used the initial and final states in the laboratory frame expressed in terms of the intrinsic states $|\phi_K>$, using the Bohr-Mottelson factorization [34].

The β-decay half-life is obtained by summing up all the allowed transition probabilities, weighed with phase space factors, up to states in the daughter nucleus with excitation energies lying within the Q-window,

$$T^{-1}_{1/2} = \frac{A^2}{D} \sum_\omega f\left(Z, \omega\right) B(GT)\,, \tag{2.8}$$

where $f\left(Z, \omega\right)$ is the Fermi integral [35] and $D = 6200$ s. We include standard effective factors

$$A^2 = \left[\left(g_A / g_V \right)_{\text{eff}} \right]^2 = \left[0.7 \left(g_A / g_V \right)_{\text{free}} \right]^2 . \tag{2.9}$$

In β^+/EC decay, $f\left(Z, \omega\right)$ consists of two parts, positron emission and electron capture. In this work we have computed them numerically for each value of the energy, as explained in Ref. [35].

III. RESULTS AND DISCUSSION

In this section we present the results obtained from the above mentioned theoretical formalism for the β-decay patterns of the neutron-deficient ^{184,186,188,190,192,194}Pb isotopes. First, we discuss the energy surfaces and shape coexistence expected in these isotopes. Then, we show on some examples the sensitivity of the Gamow-Teller strength distributions to the various ingredients in the calculation. Finally, we present the results obtained for the Gamow-Teller strength distributions with special attention to their dependence on the nuclear shape and discuss their relevance as signatures of deformation to be explored experimentally.

A. Deformation energy curves

We show in Fig. 1 the HF energies calculated with the Skyrme force Sk3 and pairing correlations treated in the fixed gap approach, for all the isotopes considered, as a function of the quadrupole deformation parameter β. The latter is defined as

$$\beta = \sqrt{\frac{\pi}{5}} \frac{Q_p}{Z < r^2 >} \tag{3.1}$$

in terms of the proton quadrupole moment Q_p and the charge r.m.s. radius $< r^2 >$. For a better comparison, the curves are scaled to the energy of their ground states and are shifted by 1,2,3,4,5 MeV for A=186,188,190,192,194, respectively. As we can see in the figure, prolate solutions corresponding to values ($\beta > 0$) are always present from A=184 to A=190, and are indeed the ground state for this choice of force and gap parameters. The prolate minimum shows only a shoulder in A=192 and disappears completely in A=194, where only the spherical solution remains. Spherical local minima can be seen in all the isotopes except for A=192, the one in A=190 being very shallow. Oblate minima ($\beta < 0$) are also present in all the isotopes except for the one closer to stability A=194. We can also see in Fig. 1 that the oblate deformation corresponding to the local oblate minima in all the isotopes is rather stable at $\beta = -0.2$, while the prolate deformation at the minima becomes larger as we remove more and more neutrons, to reach $\beta = 0.32$ in A=184. Mass deformations follow closely charge deformations.

Our results are in qualitative agreement with experiment in the sense that we find different coexisting shapes in this mass region, although they are at variance with experiment [1] in the predicted ground state shape. Experimentally, the ground states of all the isotopes considered here are found to be spherical, while we find a spherical shape as the ground state in A=194, an oblate shape in A=192 and a prolate shape in the remaining cases considered (A=184-190). This discrepancy is not surprising because as we have mentioned in the Introduction, even the more sophisticated formalisms fail in some instances [9] to account for the spherical ground state, showing an extreme sensitivity to fine details of the two-body interactions. To illustrate this sensitivity, we compare in Fig. 2 on the example of A=184, the energy deformation curves obtained when we change the force from Sk3 to SG2 and SLy4, and when we change the pairing correlations from fixed gap parameters to constant pairing interaction with $G_{\pi(\nu)}$ strengths given by Eq. (2.1). We can see in Fig. 2 that although we get a prolate ground state in all the cases considered, the calculation with a constant pairing strength (dotted line) takes the spherical minimum very close in energy to the ground state. Indeed by slightly changing the G-values (the relative values of G_π versus G_ν), we can get the spherical solution as the ground state. An analysis along these lines was made in Ref. [18] with analogous results. It is also worth mentioning that the force SLy4 produces three minima which are very close in energy.

The results shown in Fig. 2 represent what happens when using other forces and other gap parameters or pairing strength values. That is, the deformation minima remain at about the same deformation values but their relative energies may change considerably. This example is also representative of the situation with respect to other isotopes.

B. Gamow-Teller strength distributions and deformation

In this subsection we study the energy distribution of the Gamow-Teller strengths calculated at the equilibrium shapes that minimize the energy of the nucleus. First, we settle the values of the coupling strength constants of our separable residual *ph* and *pp* forces. In this work we use the same value for all the isotopes considered, which is fixed by comparison to the experimental $B^-(GT)$ strength resonance observed from (p,n) charge exchange reactions in ^{208}Pb at an energy of 19.2 MeV relative to the parent nucleus ^{208}Pb [36]. In this way, we reproduce the energy of the resonance with $\chi_{GT}^{ph} = 0.09\,(0.07)$ MeV, when using SG2 (Sk3) forces and these are the values we use here. Once the value of the *ph* spin-isospin residual force has been established, the value of the *pp* residual force is usually chosen

to reproduce the measured half-life. In the present case, we have calculated the half-lives as a function of the κ_{GT}^{pp} parameter and have found that they are very little dependent on this parameter. This is illustrated in Fig. 3, where we can see the results obtained for $T_{1/2}$ from Eqs. (2.8) and (2.9). The results correspond to the case ^{190}Pb with an experimental half-life $T_{1/2} = 71$ s. The effect of the *pp* force on the GT strength distributions can be seen in the inset, where we have plotted the distributions for the oblate and prolate shapes with $\kappa_{GT}^{pp} = 0$ and 0.02 MeV. From now on, we use $\kappa_{GT}^{pp} = 0.02$ MeV in the calculations of the GT strengths. This value is compatible with the parametrization of Ref. [31], where it was found $\kappa_{GT}^{pp} = 0.58/A^{0.7}$ MeV.

In Fig. 4 we study the influence of both the Skyrme force and the pairing treatment used on the GT strength distributions. We do that on the example of the isotope ^{184}Pb and perform the calculations for the different shapes that minimize the energy of this isotope, which are shown in Fig. 2. The purpose of this figure is to show that the different profiles obtained for different deformations remain when the force and/or pairing are changed. This implies that the GT profile is characteristic of the shape and depends little on the details of the two-body forces used. Fig. 4, as well as all the coming figures containing GT strength distributions, shows in addition to the discrete strengths, a continuous distribution resulting from a folding procedure using $\Gamma = 1$ MeV width gaussians on the discrete spectrum. The $B(GT)$ strength is plotted versus the excitation energy of the corresponding daughter nucleus. On the left panels in Fig. 4 we show the results from the oblate shape, in the middle the results from the spherical shape, and on the right panels we show those from the prolate shape. For an easier comparison between the various results, we have used in all the panels the same scales of strengths and energies. In the upper row we compare the results from two different Skyrme forces Sk3 and SG2, using pairing correlations with fixed gap parameters $\Delta_\pi = \Delta_\nu = 0.9$ MeV, as obtained from the general expression given in Sec. 2. Results from Sk3 and SG2 are plotted upward and downward, respectively. In the lower row we compare the results from Sk3 using fixed gap parameters (plotted upward) and constant pairing strengths given by Eq.(2.1) plotted downward. The main point to stress in this figure is the fact that the structure of the GT strength profiles is different for each deformation but very similar when we compare the calculation of reference (Sk3 with fixed pairing gaps) plotted upward with those plotted downward. This is specially true in the low energy region where the oblate shape gives rise to a three bump structure below 5 MeV, the spherical shape a single bump structure, and the prolate shape a two peaked structure with a first strong single peak at very low energy and a more spread second bump at higher energies.

The main difference between the calculations from Sk3 and SG2 is a small shift to lower excitation energies in the case of SG2. This is better seen in the spherical case where a single peak is present. Actually, in the strict spherical limit the fragmentation of the strength observed in the figure would collapse to single excitation energies corresponding to the transitions between degenerate spherical orbitals. The fragmentation observed arises from the small deformation present in our deformed formalism ($\beta = 0.003$), which is enough to break the degeneracy of the third components of angular momentum. The origin of the shift in the excitation energy observed with different forces, can be traced back to the predicted energies for the $h_{9/2}$ and $h_{11/2}$ spherical shells. The main contribution to the GT strength at low energies comes from the transition connecting the almost fully occupied $\pi h_{11/2}$ shell with the partially unoccupied $\nu h_{9/2}$ shell, and the relative position of the two shells (closer for SG2 than for Sk3) determines the GT excitation energy. This effect translates into the deformed cases where the non-degenerate orbitals spread around the energy of the spherical shell. The difference between the calculations with different pairing treatments shown in the lower panels is due to the different occupation probabilities of the orbitals that weigh differently the matrix elements connecting the proton and neutron states, as well as to the different quasiparticle energies that finally shift the excitation energy of the GT transitions.

In Fig. 5 we show the results for the $B(GT)$ strength distributions in $(g_A^2/4\pi)$ units, calculated within QRPA based on the force Sk3 with fixed pairing gaps and residual separable interactions *ph* and *pp* with coupling strengths given by $\chi_{GT}^{ph} = 0.07$ MeV and $\kappa_{GT}^{pp} = 0.02$ MeV, respectively. In the left panels we show the results obtained with spherical shapes from ^{184}Pb up to ^{192}Pb, the middle panels are for oblate shapes and the right panels are for prolate shapes in the same chain of isotopes. In each column we have used the same scale for the GT strength to appreciate better the changes as we increase the number of neutrons. The scale on energies is always 7 MeV, enough to include all the Q_{EC} energies, whose maximum value is $Q_{EC} = 5.84$ MeV in ^{184}Pb. We can see in this figure the progress of the profiles as we change the mass number (number of neutrons). We can see a continuous transition from the lightest (A=184) to the heaviest (A=192) isotopes, that can be guided by the dashed lines crossing the figures. Thus, we can see that the strength in the spherical case is accumulated in a resonance peaked at around 3 MeV and quite stable against the number of neutrons. This strength has its origin in the $\pi h_{11/2} \rightarrow \nu h_{9/2}$ transition. In the case of oblate shapes, we observe one peak at low energies around 2 MeV, which stays in all the isotopes although is weaker as we approach the stability. There is also a second peak clearly seen in ^{184}Pb that moves to lower energy with mass and merges with the first peak gradually. Finally, we observe a third peak that again moves to lower energy with mass. While this third peak is practically the same in all the isotopes, the two first peaks become weaker with increasing neutron number. An analysis of the structure of these transitions reveals that while the first two peaks arise from

several transitions between negative parity states (mainly from $\pi h_{11/2} \rightarrow \nu h_{9/2}$ transitions), the third peak at higher energy corresponds to transitions between positive parity states with a dominant transition $\pi(13/2)^+ \rightarrow \nu(11/2)^+$, connecting the proton $i_{13/2}$ shell with the neutron $i_{11/2}$ shell. The prolate cases show also one first peak very strong and stable at around 1 MeV, originated by a single transition, as we can see in the next figures. There is also a second peak at higher energy in ^{184}Pb. This peak is more fragmented than the lower energy peak and moves to lower energy loosing strength as we move downward in the figure. In the prolate case both peaks are originated from transitions between negative parity states, reminiscent of the transition $\pi h_{11/2} \rightarrow \nu h_{9/2}$ in the spherical case.

Now, we can particularize the discussion case by case analyzing in detail each isotope with regard to its deformation signatures. In the next figures (Figs. 6-11) we show for each isotope a comparison of the GT distributions obtained from the spherical (upper panel), oblate (middle panel) and prolate shapes (lower panel). We also show the discrete spectra, not folded, as they come directly from the QRPA calculations.

In Fig. 6 for ^{184}Pb we can see a bump between 2.5 and 3 MeV in the spherical case. In the oblate case we get a three bump structure with peaks centered at 1.5, 3, and 5 MeV, respectively. The two peaks at lower energy are fragmented within a range of 1 MeV while the third peak is little fragmented. On the contrary, in the prolate case we see a very strong single peak at 1 MeV and a second narrow peak at 3 MeV followed by a tail spread up to 5 MeV. Similarly, we can see in Figs. 7-10 the following characteristics which are common to all the isotopes: i) an accumulation of the strength between 2.5 MeV and 3 MeV, depending on the isotope, for the spherical shape; ii) a very fragmented bump structure spread from 1.5 MeV up to 3.5 MeV, as well as a single peak located between 4 MeV and 5 MeV, depending on the isotope, in the oblate case; iii) a single very strong peak at very low energy and a more spread structure beyond 3 MeV in the prolate case. Fig. 11 shows the results for ^{194}Pb, where only a stable solution, which is spherical, is found with Sk3 (see Fig. 1). The strength in this case is located beyond the Q_{EC} value and therefore of no significance from the β decay point of view. Our calculation with Sk3 predicts a stable isotope although the half-life has been measured to be $T_{1/2} = 720$ s. We shall come back to this point later on when discussing our results for half-lives.

Now we focus our attention on the isotopes ^{188,190,192}Pb, because several features combine to make them the best candidates for β-decay strength distributions measurements [22]. These features are: i) a dominant β^+/EC decay component (see Table 1); ii) a relatively large half-life ($T_{1/2} = 25 - 210$ s); and iii) a large enough Q_{EC} energy (3.3-4.5 MeV). In the case of ^{188}Pb, practically all the strength is found below its Q_{EC} value except for one peak at 4.5 MeV in the oblate case. A signature of deformation in this isotope would be the existence of GT strength below an excitation energy of 2 MeV, a region where the spherical shape does not generate any strength. If a very strong narrow peak is found in this low energy region, this would be an indication of a prolate shape, while if very fragmented strength is found this would indicate an oblate shape. The situation is similar in ^{190}Pb, but here it is even more evident the existence of three regions. Appearance of strength below 2.5 MeV would indicate again a deformed nuclear shape. If the strength were located below 1.5 MeV in the form of a narrow peak, it would indicate a prolate shape while its absence would rule out this possibility. In the case of ^{192}Pb, part of the strength is already located beyond the Q_{EC} window but still we get very clean signatures of deformation. The existence of a narrow strength distribution very close to the ground state would clearly indicate a prolate shape of the decaying nucleus and the absence of this strong peak together with the existence of strength extended up to 3 MeV indicates an oblate shape. The lack of strength below 2.5 MeV would rule out a deformed shape.

We have also calculated the half-lives (Eq. (2.8)) corresponding to the β^+/EC decays of these isotopes with the purpose of contrasting our results against the measured half-lives and checking that there is no fundamental disagreement with experiment. The β^+/EC decay mode competes in this mass region with α-decay and the relative contribution of the two decays can be seen in Table 1 as the percentage of the β^+/EC decay with respect to the total decay [28]. We can also see in Table 1 the experimental half-lives [28], as well as the calculated half-lives from the spherical, oblate and prolate shapes with the forces Sk3 and SG2, using quenching factors given in Eq. (2.9) and experimental Q_{EC} values. In principle, different Q-values should be used in the calculations for different starting/ending energy minima. Nevertheless, the Q-values calculated from the binding energies of parent and daughter are quite similar for the various shapes and close to the corresponding experimental values. We have also checked that the half-lives calculated with the experimental Q_{EC} values change in less than a factor of two when Q_{EC} is varied within 1 MeV around this value. This is at least the case in the more relevant isotopes ^{190,192}Pb, where the β^+ percentage is above 99%. One should also mention that the spherical cases are more sensitive to the Q_{EC} values because the location of the GT resonance close to the Q_{EC} value may be critical. Nevertheless, the half-lives in the spherical cases are always much larger than the corresponding to the deformed cases.

The decay of the most unstable isotopes ^{184,186}Pb are dominated by α-decay and therefore the predictions for the β^+/EC decay half-lives should be above the measured value. This is indeed observed in the table. In the case of ^{184}Pb, the β^+ percentage is small (20(15)%). Then, we expect the calculated β^+/EC half-lives to be roughly about one order of magnitude larger than the total experimental half-life and this is observed in the table. For ^{186}Pb the decay

is shared by α and β emission in comparable proportions. Thus, we expect β^+/EC half-lives of the order of twice the total half-life measured, and this is roughly the case in Table 1. We also observe a general characteristic common to all the isotopes, the spherical shape produces always the largest half-life and the prolate shape the lowest one with the oblate half-life in between. The most interesting cases are ^{188,190,192}Pb. These decays are clearly dominated by β^+/EC decay with half-lives ranging from $T_{1/2} = 25.5$ s up to $T_{1/2} = 210$ s. In ^{188}Pb the experimental $T_{1/2} = 25.5$ s, is compatible with the prolate and oblate shapes in both Sk3 and SG2. In ^{190}Pb the experimental $T_{1/2} = 71$ s, is much closer to the oblate calculation ($T_{1/2} = 83$ s) and about a factor of two larger than the prolate half-life ($T_{1/2} = 27$ s) in Sk3. The SG2 results are in this case below experiment. The measured half-life of ^{192}Pb ($T_{1/2} = 210$ s) is well reproduced by the oblate shape, but it is a factor of 8 larger than the half-life of the prolate shape in Sk3. The results from SG2 are a factor of 2 (3) below experiment for the oblate (prolate) shape. In the case of ^{194}Pb, as already indicated, the Sk3 force predicts only one minimum, which is spherical and stable against β-decay. The oblate shape corresponding to the force SG2 predicts a half-life that agrees nicely with experiment, while the half-life obtained with the spherical shape is too large.

As a general comment we can mention that the β^+/EC half-lives predicted by the spherical shapes are in general much larger than the experimental half-lives. As a consequence, even though the spherical shape corresponds experimentally to the ground state of the nucleus, according to our calculations, the β^+/EC half-lives are determined to a large extent by the β^+/EC decay of the oblate and prolate shape isomers. Within the present calculations, we would be unable to reproduce the half-lives if we would restrict ourselves to spherical shapes.

IV. CONCLUSIONS

We have studied the energy distribution of the Gamow-Teller strength in the neutron-deficient ^{184,186,188,190,192,194}Pb isotopes. The study has been done within a deformed pnQRPA formalism with spin-isospin *ph* and *pp* separable residual interactions. The quasiparticle mean field includes pairing correlations in BCS approximation and it is generated from a deformed HF approach with two-body Skyrme effective interactions.

The parameters of the Skyrme forces are previously determined by fits to nuclear matter and ground state properties of spherical nuclei and the pairing gap parameters are extracted from the experimental masses. The equilibrium deformation is derived self-consistently within the HF procedure. The coupling strength of the *ph* residual interaction is fixed to reproduce the energy of the GT resonance in ^{208}Pb. The value obtained is close to the coupling strength derived consistently from the Skyrme force. Finally, the coupling strength of the *pp* residual interaction is taken from existing global parametrizations, although we find our results to be quite insensitive to this value. Our calculation has basically no free parameters to fit locally any of the particular isotopes discussed.

Although the present procedure to generate the structure properties may be enough for a first estimate of the GT strength distributions, it would be interesting in the future to improve this description and discuss the effect of using the most recent Skyrme forces available in the literature together with a treatment of the pairing correlations using zero-range density dependent pairing interactions, where issues such as renormalization or regularization of the pairing force can be analyzed in this context.

We have investigated the sensitivity of our results to the forces used and we arrive to the following conclusions: i) In a given isotope, the energy deformation curve and, in particular, the relative energies of the spherical, oblate, and prolate minima, are very sensitive to the Skyrme and pairing forces used. The ground state shape predicted may be modified with different choices for these forces. Nevertheless, the qualitative behavior of the energy profile in each isotope remains unchanged against changes in the Skyrme and pairing forces in the sense that the deformations at which the minima occur are hardly shifted and that the shape coexistence between spherical, oblate and prolate shapes is a constant feature in the more neutron deficient isotopes. ii) The GT strength distributions calculated at the equilibrium deformations show specific characteristics for each deformation that remain against changes of the Skyrme and pairing forces. The effect of the deformation on the GT strength distributions is much stronger than the effects coming from the Skyrme or pairing forces used. iii) As a consequence, we have been able to identify clear signatures of deformation on the GT strength distributions of the Pb isotopes studied. These signatures are related to the profiles of the GT strength distributions, which are peaked at different energies depending on the shape of the decaying nucleus. A detailed analysis of the best candidates to be measured, ^{188,190,192}Pb, has been performed and the characteristic features of their GT strength distributions have been identified.

The calculated β^+/EC half-lives show a strong dependence on the shape of the nucleus. The spherical shape produces always the largest half-life, which is far away from experiment. The prolate shape gives the lowest one while the oblate half-life lies in between and agrees better with experiment. The conclusion from our calculated half-lives is that in order to reproduce the experimental β^+/EC half-lives, the decay of the spherical isomer is not enough and one has to consider the decay of the oblate and prolate shape isomers as well.

Acknowledgments

We are grateful to A. Algora and B. Rubio for useful discussions. This work was supported by Ministerio de Educación y Ciencia (Spain) under contract number BFM2002-03562. Two of us (O.M. and R.A.-R.) thank Ministerio de Educación y Ciencia (Spain) for financial support.

---

[1] R. Julin, K. Helariutta and M. Muikku, J. Phys. G.: Nucl. Part. Phys. **27**, R109 (2001).
[2] J. Heese, K.H. Maier, H. Grawe, J. Grebosz, H. Kluge, W. Meczynski, M. Schramm, R. Schubart, K. Sphor and J. Styczen, Phys. Lett. B **302**, 390 (1993).
[3] A.N. Andreyev *et al.*, Nature **405**, 430 (2000).
[4] G.D. Dracoulis, A.P. Byrne and A.M. Baxter, Phys. Lett. B **432**, 37 (1998).
[5] K. Heyde, J. Schietse and C. de Coester, Phys. Rev. C **44**, 2216 (1991).
[6] R. Bengtsson and W. Nazarewicz, Z. Phys. A **334**, 269 (1989).
[7] W. Nazarewicz, Phys. Lett. B **305**, 195 (1993).
[8] N.A. Smirnova, P.-H. Heenen and G. Neyens, Phys. Lett. B **569**, 151 (2003).
[9] T. Niksic, D. Vretenar, P. Ring and G.A. Lalazissis, Phys. Rev. C **65**, 054320 (2002).
[10] T. Duguet, M. Bender, P. Bonche and P.-H. Heenen, Phys. Lett. B **559**, 201 (2003).
[11] J.L. Egido, L.M. Robledo and R.R. Rodríguez-Guzmán, Phys. Rev. Lett. **93**, 082502 (2004); R.R. Rodríguez-Guzmán, J.L. Egido and L.M. Robledo, Phys. Rev. C **69**, 054319 (2004).
[12] M. Bender, P. Bonche, T. Duguet and P.-H. Heenen, Phys. Rev. C **69**, 064303 (2004).
[13] J.L. Wood, K. Heyde, W. Nazarewicz, M. Huyse and P. Van Duppen, Phys. Rep. **215**, 101 (1992).
[14] P. Van Duppen, M. Huyse and J.L. Wood, J. Phys. G: Nucl. Part. Phys. **16**, 441 (1990).
[15] S. Yoshida, S.K. Patra, N. Takigawa and C.R. Praharaj, Phys. Rev. C **50**, 1398 (1994).
[16] M.S. Mehta, T.K. Jha, S.K. Patra and R. Gupta, nucl-th/0401021.
[17] S. Yoshida and N. Takigawa, Phys. Rev. C **55**, 1255 (1997).
[18] N. Tajima, H. Flocard, P. Bonche, J. Dobaczewski and P.-H. Heenen, Nucl. Phys. A **551**, 409 (1993).
[19] F. Frisk, I. Hamamoto and X.Z. Zhang, Phys. Rev. C **52**, 2468 (1995); I. Hamamoto and X.Z. Zhang, Z. Phys. A **353**, 145 (1995).
[20] P. Sarriguren, E. Moya de Guerra, A. Escuderos and A.C. Carrizo, Nucl. Phys. A **635**, 55 (1998); P. Sarriguren, E. Moya de Guerra and A. Escuderos, Nucl. Phys. A **658**, 13 (1999); Nucl. Phys. A **691**, 631 (2001); Phys. Rev. C **64**, 064306 (2001).
[21] E. Poirier *et al.*, Phys. Rev. C **69**, 034307 (2004); E. Nácher *et al.*, Phys. Rev. Lett. **92**, 232501 (2004).
[22] A. Algora, B. Rubio and W. Gelletly, private communication.
[23] M. Beiner, H. Flocard, N. Van Giai and P. Quentin, Nucl. Phys. A **238**, 29 (1975).
[24] N. Van Giai and H. Sagawa, Phys. Lett. B **106**, 379 (1981).
[25] P. Sarriguren, E. Moya de Guerra, and R. Nojarov, Phys. Rev. C **54**, 690 (1996).
[26] A. Chabanat, P. Bonche, P. Haensel, J. Meyer, and R. Schaeffer, Nucl. Phys. A **635**, 231 (1998).
[27] H. Flocard, P. Quentin, A.K. Kerman and D. Vautherin, Nucl. Phys. A **203**, 433 (1973).
[28] G. Audi, O. Bersillon, J. Blachot and A.H. Wapstra, Nucl. Phys. A **729**, 3 (2003).
[29] J. Krumlinde and P. Moeller, Nucl. Phys. A **417**, 419 (1984); P. Moeller and J. Randrup, Nucl. Phys. A **514**, 1 (1990).
[30] M. Hirsch, A. Staudt, K. Muto and H.V. Klapdor-Kleingrothaus, Nucl. Phys. **A535**, 62 (1991).
[31] H. Homma, E. Bender, M. Hirsch, K. Muto, H.V. Klapdor-Kleingrothaus and T. Oda, Phys. Rev. C **54**, 2972 (1996).
[32] K. Muto, E. Bender, T. Oda and H.V. Klapdor-Kleingrothaus, Z. Phys. A **341**, 407 (1992).
[33] J. Engel, P. Vogel and M.R. Zirnbauer, Phys. Rev. C **37**, 731 (1988); V.A. Kuz'min and V.G. Soloviev, Nucl. Phys. A **486**, 118 (1988).
[34] A. Bohr and B. Mottelson, *Nuclear Structure*, (Benjamin, New York 1975).
[35] N.B. Gove and M.J. Martin, Nucl. Data Tables **10**, 205 (1971).
[36] C. Gaarde et al. Nucl. Phys. A **369**, 258 (1981); *ibid.* **396**, 127c (1983).

TABLE I. Percentage of the β^+/EC involved in the total decay of the Pb isotopes, experimental [28] and theoretical half-lives [s], obtained with the forces Sk3 and SG2. Experimental Q_{EC} values have been used.

A	% (β^+/EC)	$T_{1/2}^{\text{total}}$ exp	$T_{1/2}^{\beta^+}$ (Sk3)			$T_{1/2}^{\beta^+}$ (SG2)		
			oblate	prolate	spherical	oblate	prolate	spherical
194	100	720 (30)	-	-	stable	642	-	2053
192	99.9941 (7)	210 (6)	207	28	4385	132	84	763
190	99.60 (4)	71 (1)	83	27	344	53	12	195
188	90.7 (8)	25.5 (1)	32	18	85	24	22	62
186	60 (8)	4.82 (3)	15.4	7.7	47	8.2	6.2	16
184	20 (15)	0.490 (25)	6.4	3.3	22	4.5	3.2	6.7

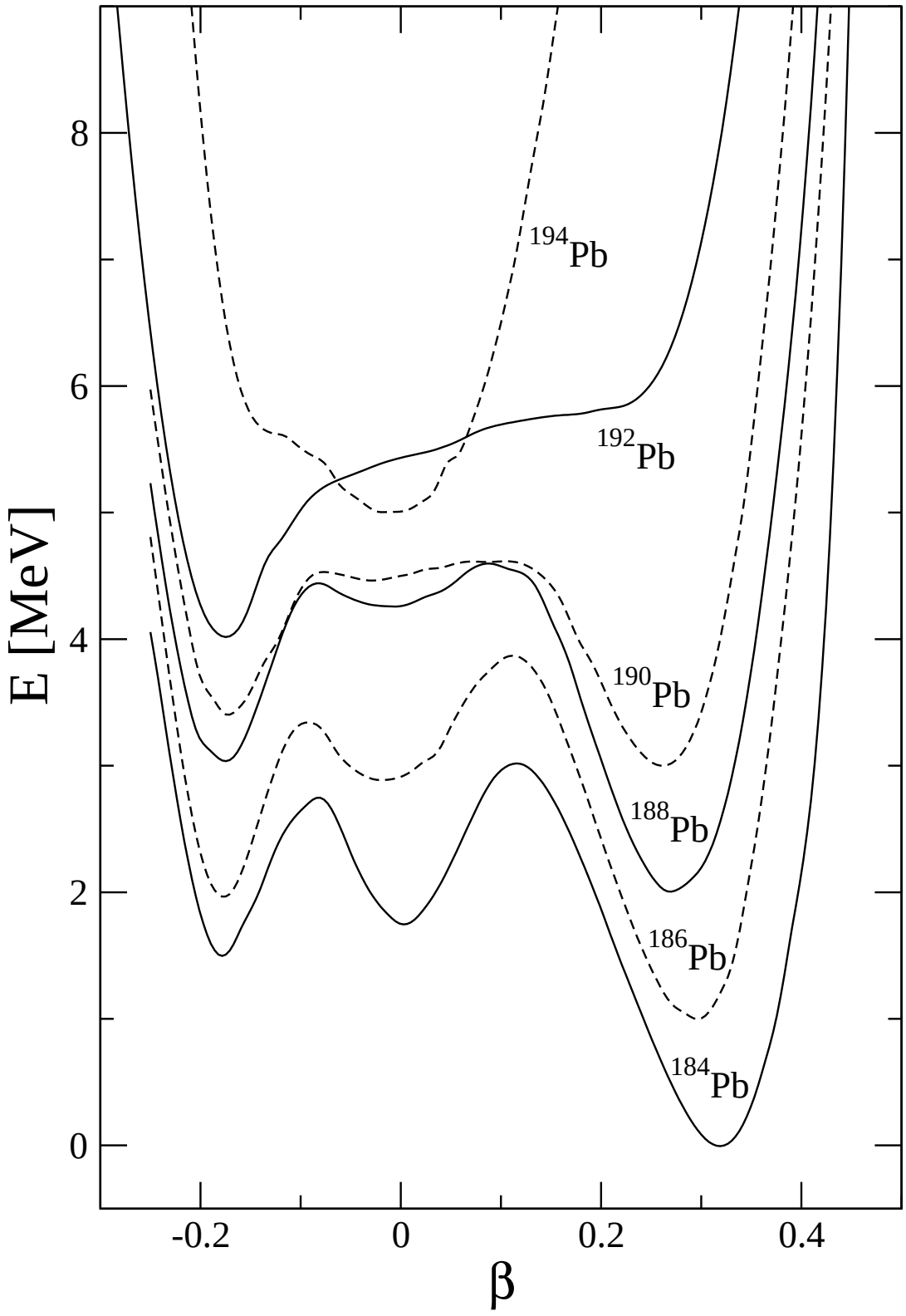

FIG. 1. HF energy of the isotopes ^{184,186,188,190,192,194}Pb obtained from constrained HF+BCS calculations with the force Sk3 and fixed pairing gap parameters as a function of the quadrupole deformation β.

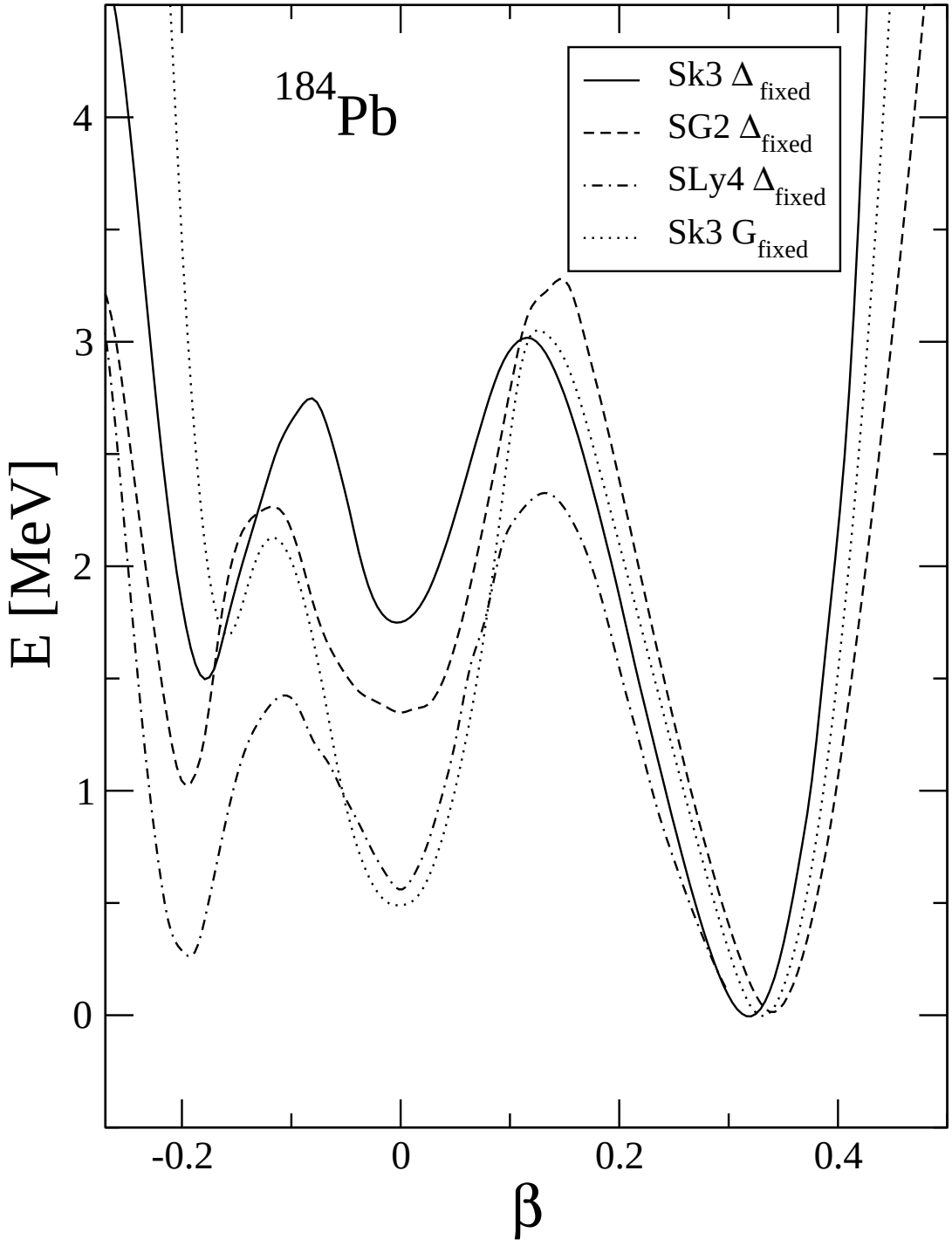

FIG. 2. HF energy of ^{184}Pb as a function of the quadrupole deformation β, for various forces and pairing treatments.

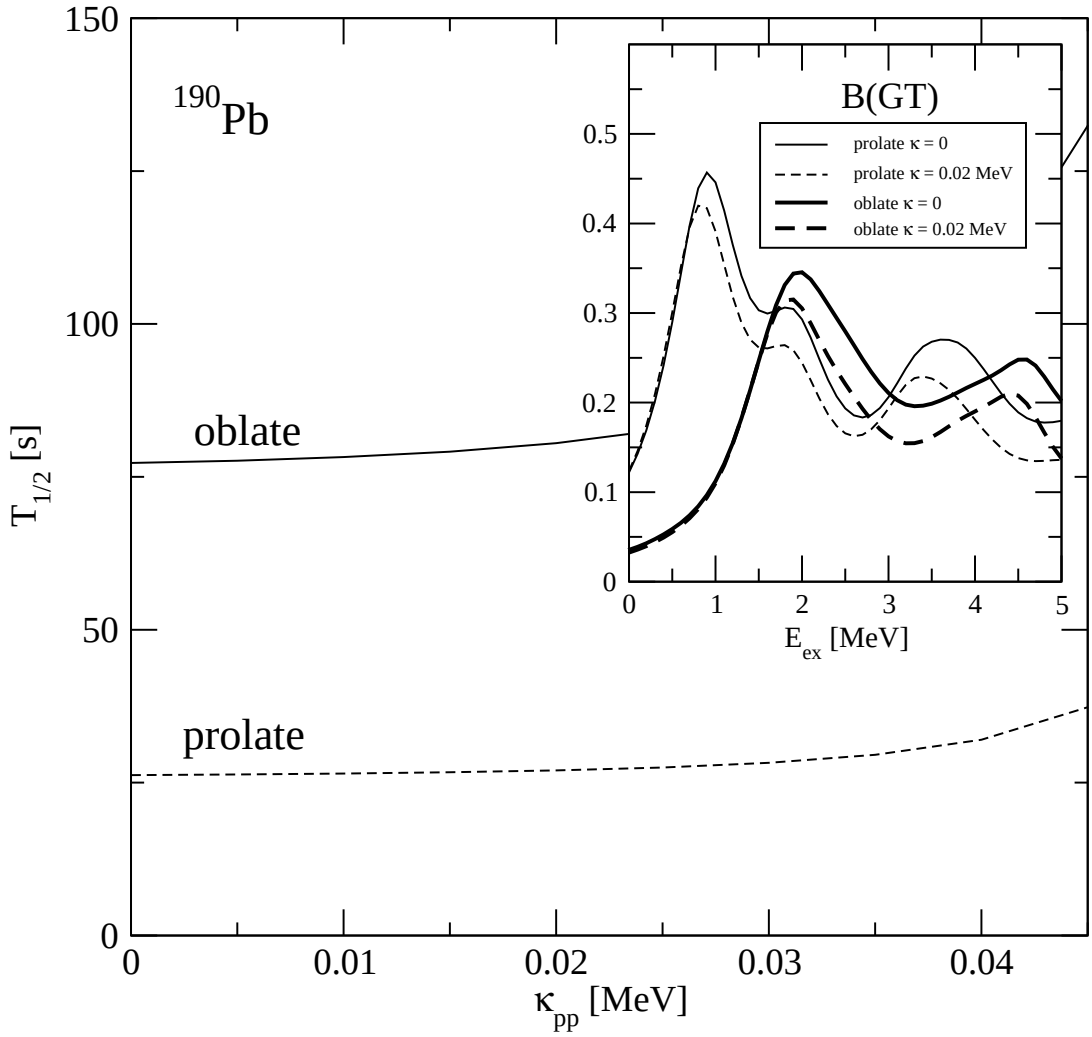

FIG. 3. Half-lives for the oblate and prolate shapes of ^{190}Pb as a function of the coupling strength of the particle-particle residual interaction κ_{pp}. In the inset we can see the $B(GT)$ strength as a function of the excitation energy for various shapes and κ_{pp} parameters.

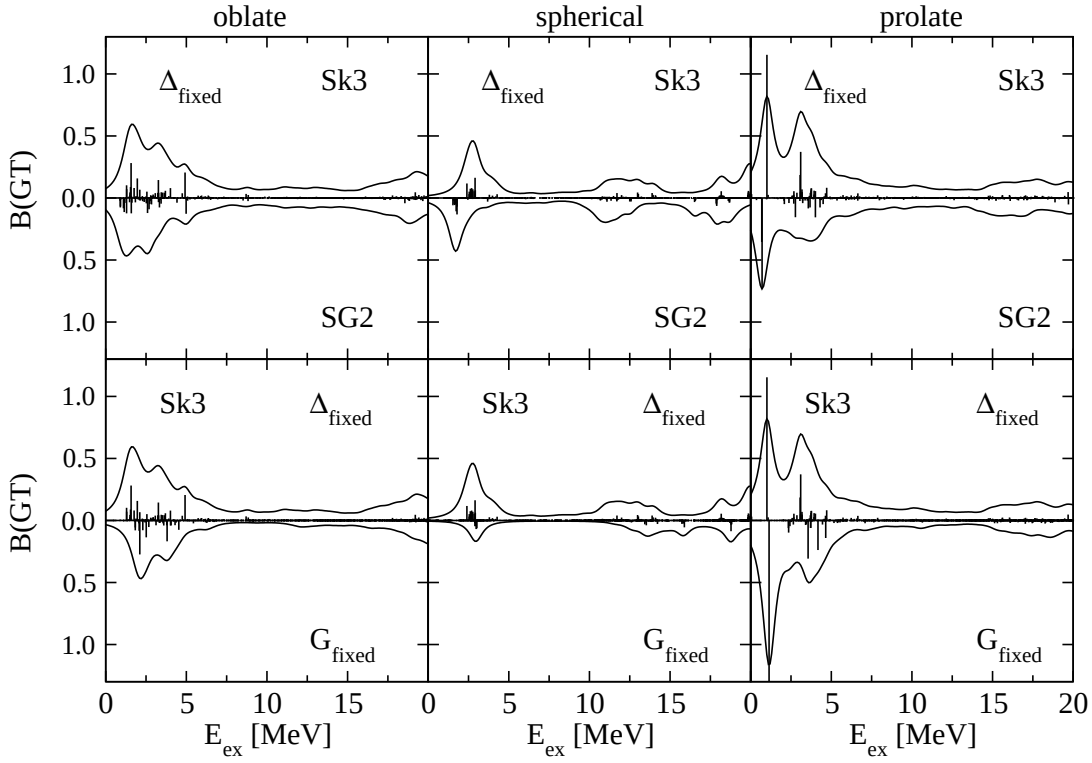

FIG. 4. Gamow-Teller strength distributions in ^{184}Pb as a function of the excitation energy in the daughter nucleus. From left to right panels we show the results for oblate, spherical, and prolate shapes. In the upper panels we show the results from Sk3 (upward) and SG2 (downward) with fixed gap parameters, while in the lower panels we show the results from fixed pairing gaps (upward) and constant pairing strengths (downward) for Sk3.

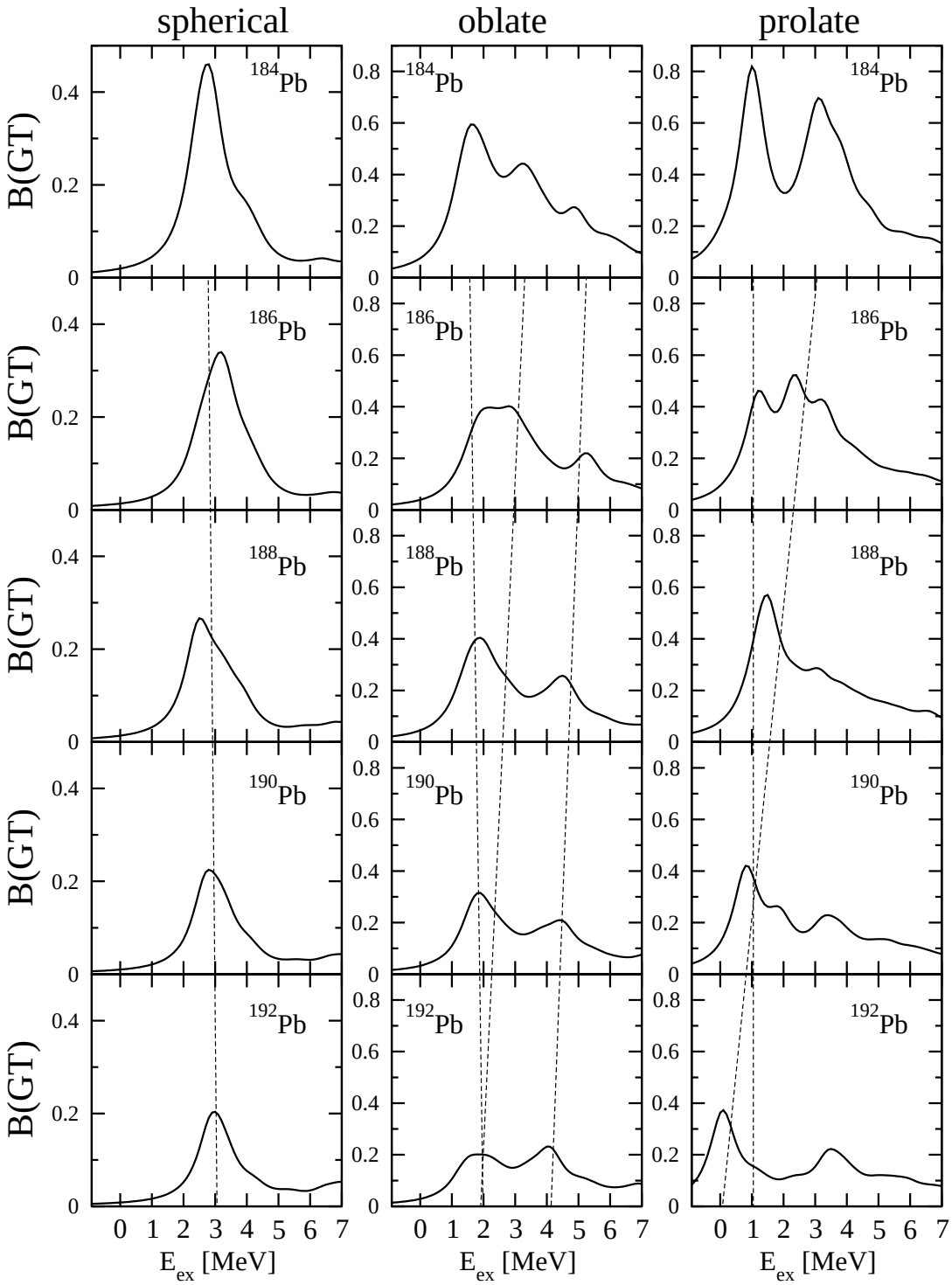

FIG. 5. Gamow-Teller strength distributions in the ^{184,186,188,190,192}Pb isotopes for spherical (left), oblate (middle) and prolate (right) shapes. Results are obtained from Sk3 force with fixed gap parameters.

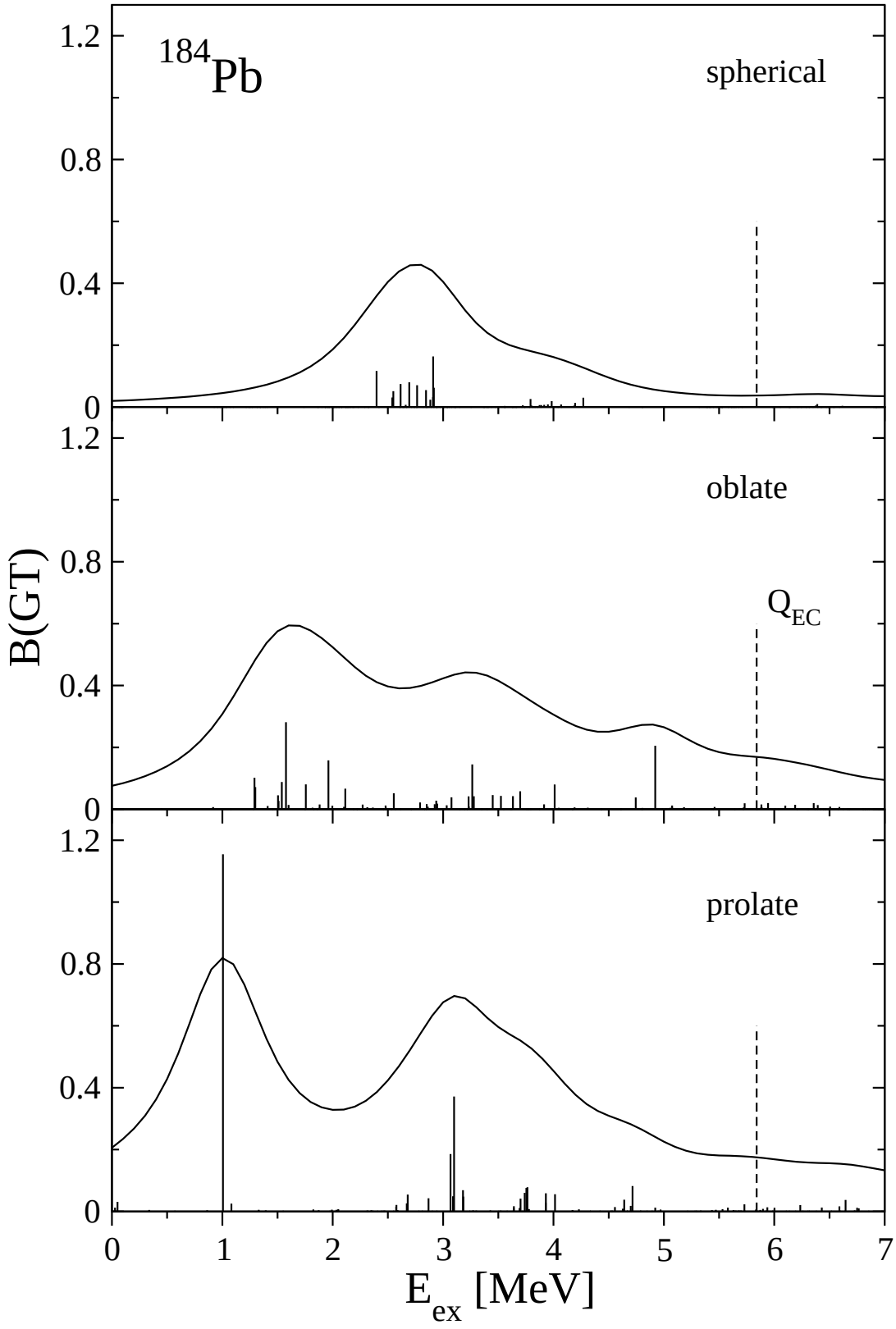

FIG. 6. Gamow-Teller strength distributions (discrete and folded) in ^{184}Pb. The experimental Q_{EC} energy is shown with a dashed vertical line.

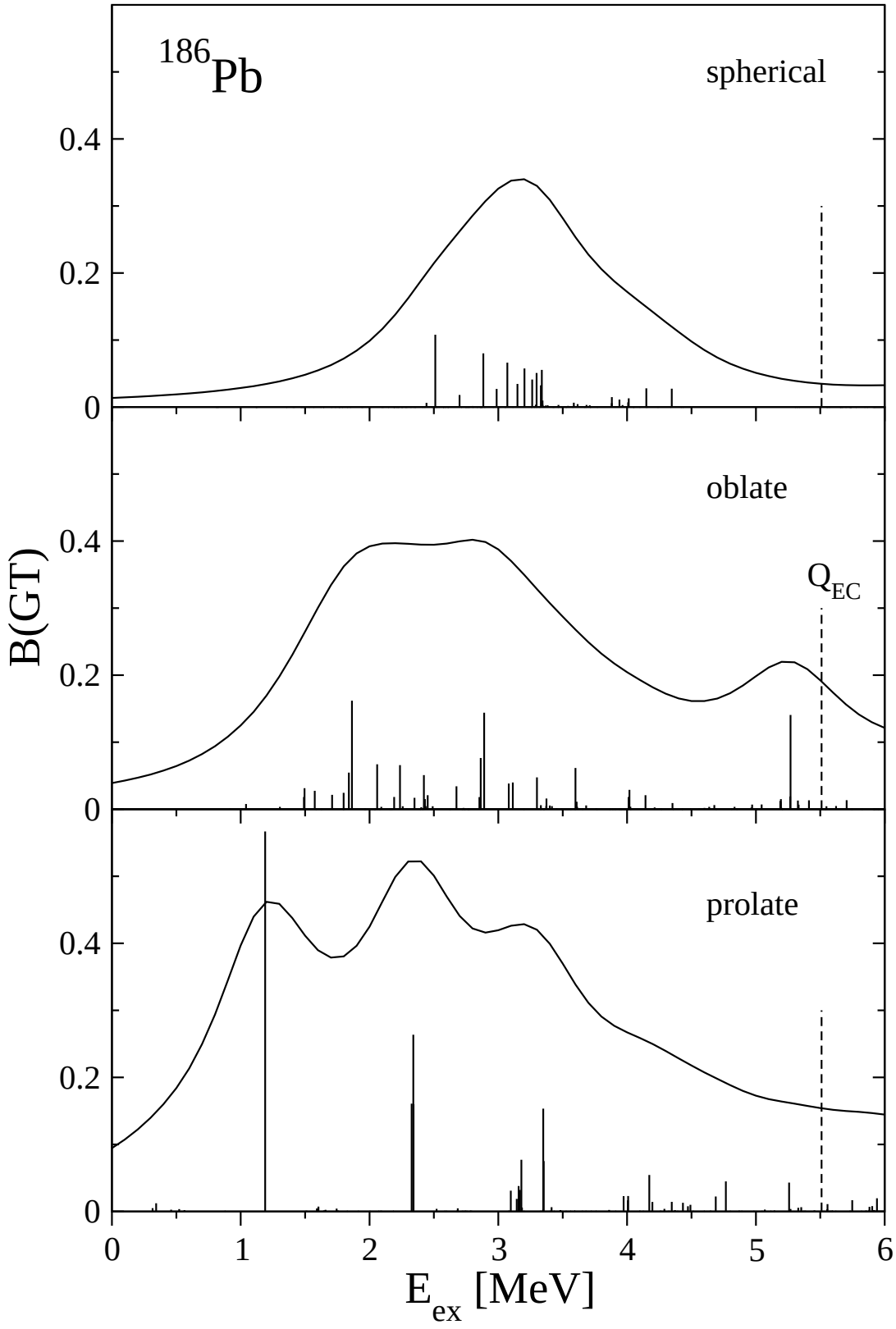

FIG. 7. Same as in Fig. 6 for ^{186}Pb.

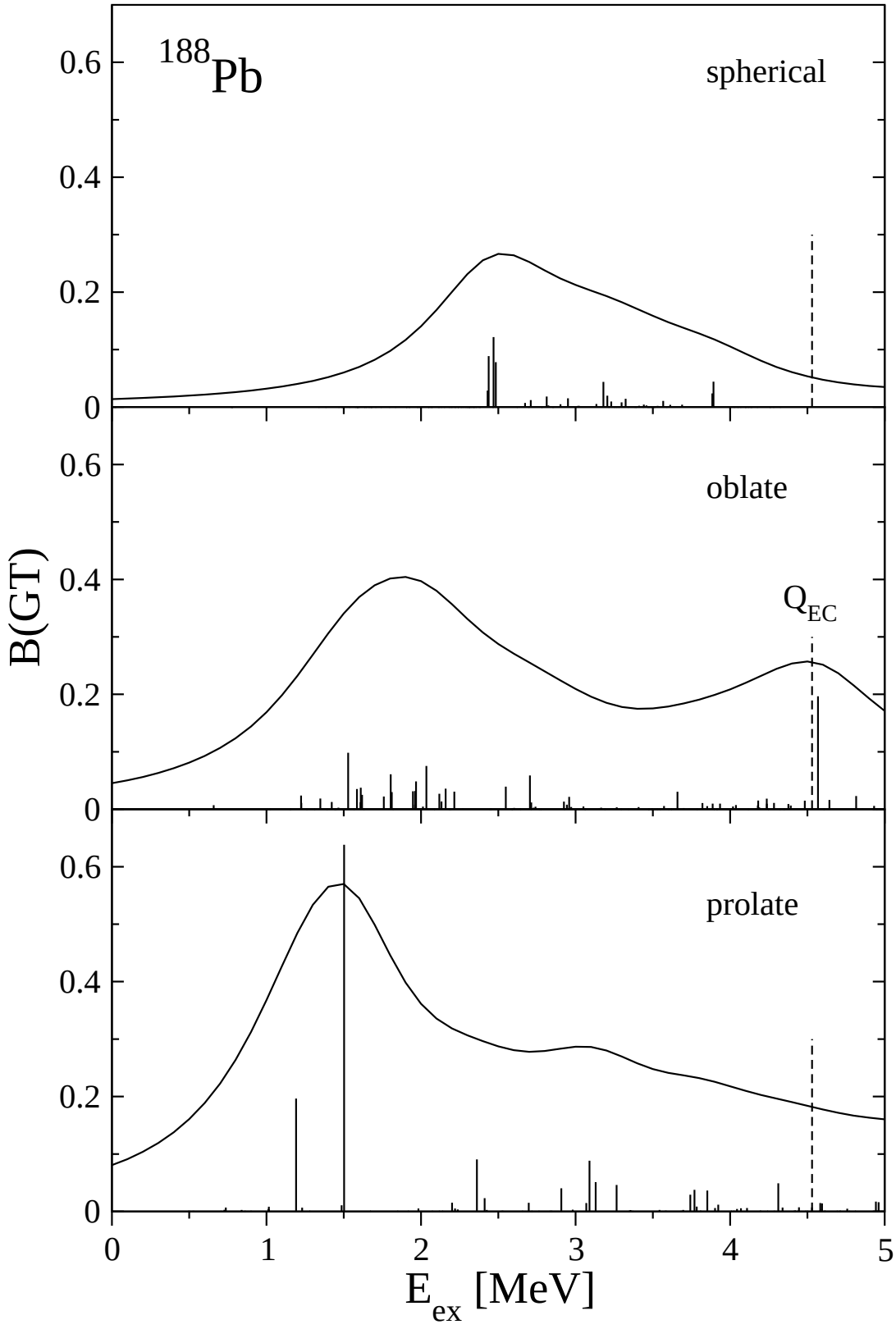

FIG. 8. Same as in Fig. 6 for ^{188}Pb.

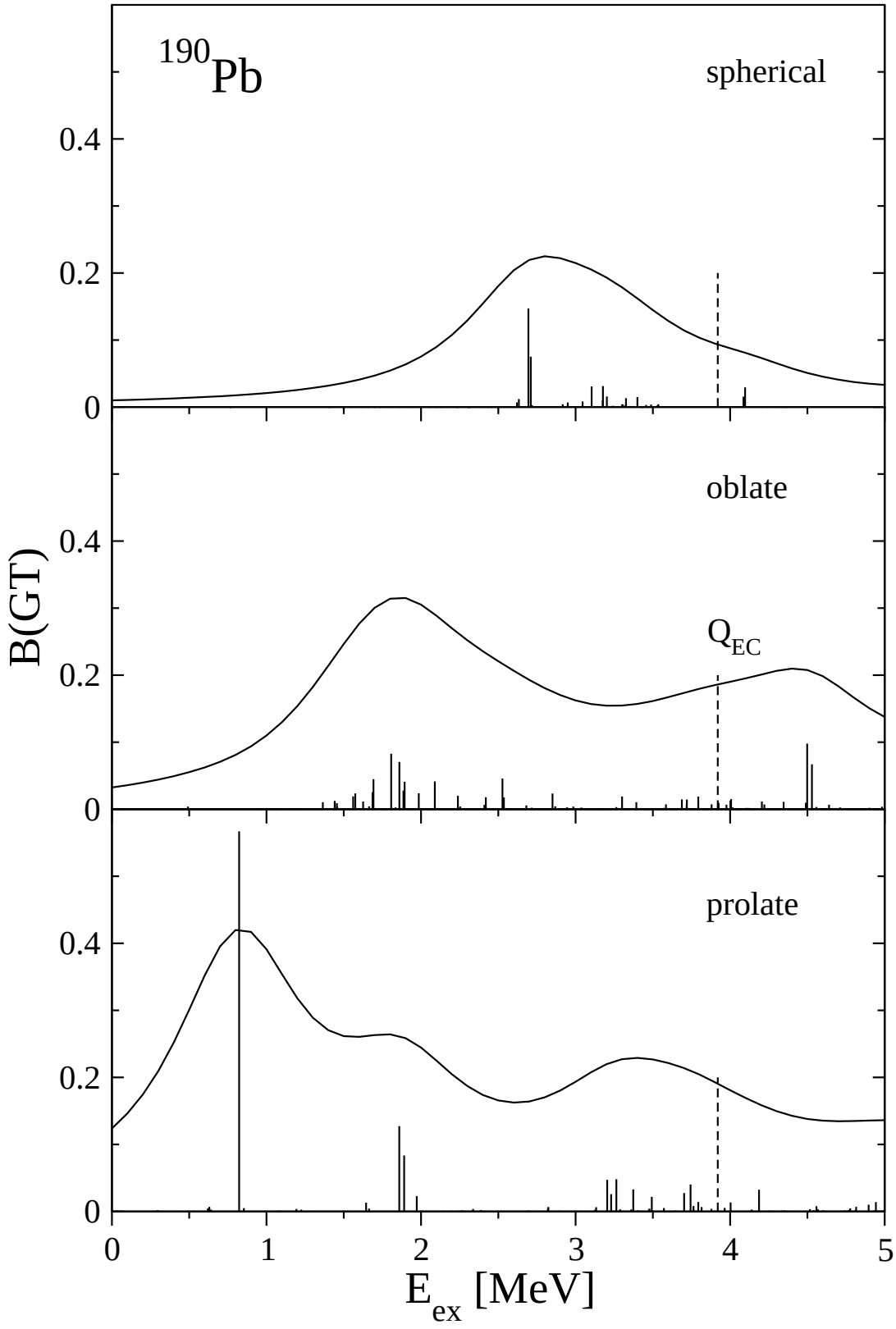

FIG. 9. Same as in Fig. 6 for ^{190}Pb.

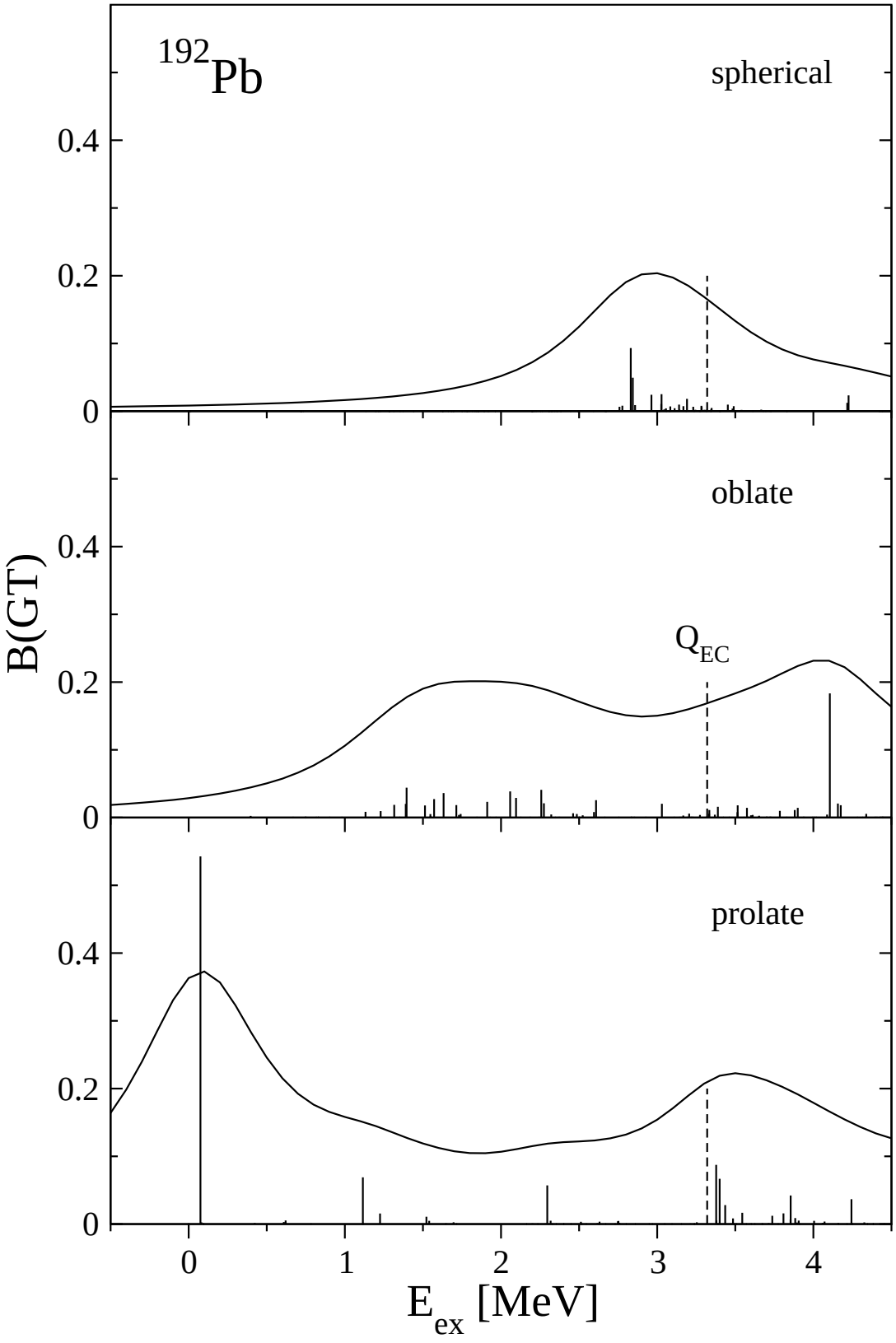

FIG. 10. Same as in Fig. 6 for ^{192}Pb.

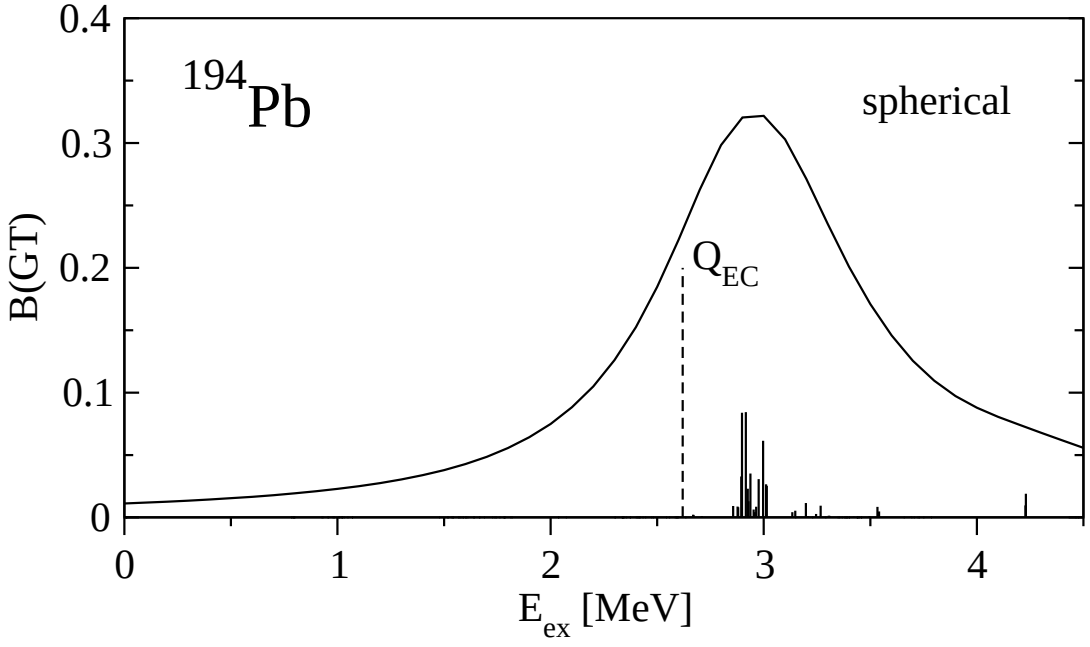

FIG. 11. Same as in Fig. 6 for ^{194}Pb.